Acta Crystallographica Section D
Biological Crystallography
ISSN 0907-4449

A neutron crystallographic analysis of a rubredoxin mutant at 1.6 Å resolution

Toshiyuki Chatake,[a] Kazuo Kurihara,[a] Ichiro Tanaka,[a] Irina Tsyba,[b] Robert Bau,[b]* Francis E. Jenney Jr,[c] Michael W. W. Adams[c]* and Nobuo Niimura[a,d]*

[a]Neutron Structural Biology Group, Advanced Science Research Center, Japan Atomic Energy Research Institute, Tokai, Ibaraki 319-1195, Japan, [b]Department of Chemistry, University of Southern California, Los Angeles, CA 90089, USA, [c]Department of Biochemistry, University of Georgia, Athens, GA 30602, USA, and [d]Department of Technology, University of Ibaraki, Hitachi, Ibaraki 316-8511, Japan

Correspondence e-mail: bau@usc.edu, adams@bmb.uga.edu, niimura@mx.ibaraki.ac.jp

Received 15 October 2003
Accepted 14 May 2004

PDB References: mutant rubredoxin, X-ray analysis, 1iu5, r1iu5sf; neutron analysis, 1iu6, r1iu6sf.

A neutron diffraction study has been carried out at 1.6 Å resolution on a mutant rubredoxin from *Pyrococcus furiosus* using the BIX-3 single-crystal diffractometer at the JRR-3 reactor of the Japan Atomic Energy Research Institute. In order to study the unusual thermostability of rubredoxin from *P. furiosus* (an organism that grows optimally at 373 K), the hydrogen-bonding patterns were compared between the wild-type protein and a 'triple-mutant' variant. In this mutant protein, three residues were changed (Trp3→Tyr3, Ile23→Val23, Leu32→Ile32) so that they are identical to those in a mesophilic rubredoxin from *Clostridium pasteurianum*. In the present study, some minor changes were found between the wild-type and mutant proteins in the hydrogen-bonding patterns of the Trp3/Tyr3 region. In this investigation, the H/D-exchange ratios in the protein were also studied. Because the target protein was soaked in D_2O during the crystallization procedure, most of the N—H and O—H bonds have become deuterated, while essentially all of the C—H bonds have not. In particular, the H/D-exchange pattern of the N—H amide bonds of the protein backbone is of interest because it may contain some indirect information about the mechanism of unfolding of this small protein. The results are in broad agreement with those from solution NMR studies, which suggest that the backbone amide bonds near the four Cys residues of the FeS_4 redox center are most resistant to H/D exchange. Finally, the detailed geometries of the water molecules of hydration around the rubredoxin molecule are also reported. The 1.6 Å resolution of the present neutron structure determination has revealed a more detailed picture than previously available of some portions of the water structure, including ordered and disordered O—D bonds. Crystallographic details: space group $P2_12_12_1$ (orthorhombic), unit-cell parameters a = 34.48, b = 35.70, c = 43.16 Å; final agreement factors R = 0.196 and R_{free} = 0.230 for 19 384 observed and 6548 unique neutron reflections collected at room temperature; crystal size 4 mm^3; a total of 423 non-H atoms, 290 H atoms and 88 D atoms were located in this study.

1. Introduction

Proteins from hyperthermophilic microorganisms are especially interesting because of their unusual thermostability. Studies of their properties are important both for understanding how such proteins can survive in such severe environments and also for providing fundamental information on mechanisms that lead to dramatic changes in protein stability. *Pyrococcus furiosus* is an anaerobic sulfur-reducing archaebacterium that is found near submarine geothermal vents on the ocean floor, with an optimal growth temperature near 373 K (Fiala & Stetter, 1986). Rubredoxin is a small

protein that consists of 53 amino-acid residues containing a single redox-active $Fe(SCys)_4$ center. Rubredoxin from *P. furiosus* (PfRd) can maintain its native structure at high temperatures (373 K). In contrast, rubredoxin from the mesophile *Clostridium pasteurianum* (CpRd), whose optimal growth temperature is 310 K, is much less stable than PfRd in spite of a 58% identity in the primary amino-acid sequences of the two proteins (Fig. 1) (Mathieu *et al.*, 1992; Blake *et al.*, 1991). It has been speculated that one possible contributor to the thermostability of PfRd might be its hydrophobic core. This is composed of eight residues: Trp3, Tyr10, Tyr12, Ile23, Phe29, Leu32 and Phe48 (shown in red in Fig. 1). In CpRd, three of these residues are different (Trp3→Tyr3, Ile23→Val23 and Leu32→Ile32). Here, we investigate the properties of a mutant of PfRd in which the above three mutations have been introduced, a protein which is significantly less stable than the wild-type PfRd at low pH. Recent NMR analyses of wild-type PfRd showed that the hydrophobic core is not the dominant contributor to this difference: no striking difference was found between this mutant rubredoxin and the wild-type protein from the NMR investigation (Zartler *et al.*, 2001). A comparison between the X-ray structures of PfRd and CpRd did not yield an unambiguous explanation for the thermostability difference either, even though the structures of PfRd and CpRd have both been determined to high resolution: 0.95 and 1.1 Å, respectively (Bau *et al.*, 1998; Dauter *et al.*, 1996). In an X-ray analysis it is usually difficult to determine hydrogen positions accurately, while a neutron crystallographic analysis can locate the H atoms even at medium resolution (1.5–2.0 Å; Shu *et al.*, 2000; Habash *et al.*, 2000; Niimura *et al.*, 1997; Kossiakoff *et al.*, 1992; Bon *et al.*, 1999; Harrison *et al.*, 1988). Thus, one of the original motivations for this project was the hope that a detailed knowledge of the hydrogen positions obtained *via* neutron diffraction might reveal some hints regarding the thermostabilization mechanism of PfRd, because H atoms influence the stability of a protein *via* the formation of hydrogen bonds.

In the present study, the hydrogen positions in the protein and water molecules of a mutant of PfRd (mut-PfRd) having three point mutations (Trp3→Tyr3, Ile23→Val23 and Leu32→Ile32) were investigated by neutron and X-ray diffraction techniques, both carried out at room temperature. The X-ray analysis, which determined the non-hydrogen structure of mut-PfRd, was necessary because it provided the initial room-temperature structural model for the neutron analysis. The neutron experiment was carried out using a new single-crystal neutron diffractometer (BIX-3) at the Japan Atomic Energy Research Institute (Tanaka *et al.*, 2002). In BIX-3, the white beam generated from a nuclear reactor is monochromated by an elastically bent perfect silicon monochromator to enhance the flux of the neutron beam at the sample position (Tanaka *et al.*, 1999). Moreover, BIX-3 is equipped with a large cylindrical neutron imaging plate as a detector (Niimura *et al.*, 1994), which can collect a large number of reflections simultaneously. Diffraction data to a resolution of 1.6 Å were collected within one month, a relatively short period of time by neutron diffraction standards. In the present study, we succeeded in determining almost all of the hydrogen and deuterium positions in mut-PfRd. Previously, we had solved the neutron crystal structure of wild-type PfRd at 1.5 Å resolution, also using the BIX-3 diffractometer (Kurihara *et al.*, 2001, 2004). In this paper, we describe three sets of results: (i) we show a comparison between the two neutron structures (PfRd and mut-PfRd), (ii) we map out the H/D distributions of the backbone N—H bonds obtained after partial H/D exchange by exposing the protein solution to D_2O and (iii) we describe the detailed appearance of water molecules of hydration near the surface of the protein.

2. Materials and methods

2.1. Sample preparation and crystallization

The triple mutant form of PfRd was produced in *Escherichia coli* and purified as reported previously (Jenney & Adams, 2001). It was crystallized from D_2O solution to reduce the incoherent scattering by the H atoms in the crystal. Large crystals of mut-PfRd, partially deuterated in this manner, were grown under the same conditions as those used for wild-type PfRd: *i.e.* using 3.6 *M* sodium/potassium phosphate (in D_2O) as a precipitant with seeding (Bau *et al.*, 1998; Kurihara *et al.*, 2001).

2.2. X-ray analysis

Prior to the neutron analysis, we solved the X-ray crystal structure of mut-PfRd so that we would have a room-temperature initial model for the neutron analysis. A large crystal was cut up into smaller pieces, one of which (having a size of 0.1 mm^3) was sealed with D_2O mother liquor into a quartz capillary. The X-ray data collection was carried out at 293 K by the oscillation method on a DIP-2020 diffractometer (MacScience Inc.) using Cu $K\alpha$ radiation generated by a rotating-anode generator at 50 kV and 120 mA. A total of 100 oscillation images were collected with an oscillation angle of 2.0° and an overlap angle of 1.0°. The set of 38 773 diffraction intensities was indexed and integrated up to 1.5 Å resolution by the program *DENZO* (Otwinowski & Minor, 1997) and scaled and merged into 8876 independent reflections with an R_{merge} value of 7.7% by the program *SCALEPACK* (Otwinowski & Minor, 1997). The space group was determined to be $P2_12_12_1$, with unit-cell parameters a = 34.48, b = 35.70, c = 43.16 Å. Initial phases were derived by the molecular-replacement method using the coordinates from the low-temperature X-ray structure of PfRd (Bau *et al.*, 1998) with

Figure 1
Sequence alignment of rubredoxins from *C. pasterurianum* (CpRd; Mathieu *et al.*, 1992), *P. furiosus* (PfRd; Blake *et al.*, 1991) and the present mutant (mut-PfRd). Underlined residues are those that differ between PfRd and CpRd. The red characters are residues involved in the hydrophobic core. The three arrows refer to residues which have been mutated from wild-type PfRd to mut-PfRd.

Table 1
Statistics of X-ray and neutron data-collection and refinement.

Values in parentheses are for the outer shell (1.66–1.60 Å for the neutron analysis and 1.55–1.50 Å for the X-ray analysis).

	Neutron	X-ray
Data collection		
Space group	$P2_12_12_1$	
Unit-cell parameters (Å)	a = 34.48, b = 35.70, c = 43.16	
Beam port/radiation	1G, JRR-3M	Cu $K\alpha$
Wavelength (Å)	2.35 ($\Delta\lambda/\lambda$ = 0.015)	1.5418
Diffractometer	BIX-3	DIP-2000
Temperature (K)	293	299
Time (d)	30	2
Maximum resolution (Å)	1.6	1.5
Observed reflections	19385	38773
Unique reflections	6584	8876
Redundancy	2.9 (1.9)	4.4 (4.3)
Completeness (%)	87.5 (66.0)	98.6 (97.7)
$I > 3\sigma(I)$ (%)	80.2 (54.3)	88.3 (69.9)
$R_{\rm merge}$ (%)	9.1 (25.4)	7.7 (19.0)
Refinement		
Resolution (Å)	10–1.6	10–1.5
R factor (%)	19.6	18.9
$R_{\rm free}$ (%)	23.0	20.4
R.m.s.d. bonds (Å)	0.007	0.007
R.m.s.d. angles (°)	1.6	1.4
Average coordinate error† (Å)	0.18	0.16
No. non-H atoms	423	434
No. H atoms	290	—
No. D atoms	88	—
No. water molecules	31	53
PDB code	1iu6	1iu5

† Estimated from a Luzzati plot (Luzzati, 1952).

the program *AMoRe* (Navaza, 1994). The mutated residues (Tyr3, Val23 and Ile32) were found in a difference Fourier map on a graphics workstation using the program *O* (Jones *et al.*, 1991) and incorporated into the structure. At the C-terminus, the electron densities of two of the residues were so poor that they were excluded from the molecular structure. After repeated model building on a graphics workstation and atomic coordinate refinement with the programs *X-PLOR* (Brünger, 1992) and *CNS* (Brünger *et al.*, 1998), one Fe atom and 53 water molecules were included in the model. The final X-ray crystal structure determination was completed with an R factor of 18.7% ($R_{\rm free}$ = 20.3%). The statistics of the X-ray data collection and structure determination are summarized in Table 1.

2.3. Neutron analysis

For the neutron experiment, the largest crystal available to us (4 mm^3) was used. The neutron diffraction experiments were performed using the BIX-3 diffractometer described earlier (Tanaka *et al.*, 1999, 2002; Niimura *et al.*, 1994). The neutron beam size is φ = 5 mm and its wavelength is 2.35 Å ($\Delta\lambda/\lambda$ = 0.015). A step-scan data-collection method with an interval of 0.3° between frames was used in order to obtain a high signal-to-noise ratio and 335 still frames were taken with the crystal mounted along the c axis. In order to collect reflections missed by the 'blind region' of the first set of frames, another data set of 340 frames was collected with the crystal mounted along a different rotation axis. Exposure times were about 1 h per frame and the total time required for the two data sets was 30 d. The diffraction patterns on the neutron imaging plate were processed up to 1.6 Å with the programs *DENZO* and *SCALEPACK* (Otwinowski & Minor, 1997), both of which were suitably modified for the processing of neutron diffraction data (these modifications took into account the cylindrical shape of the neutron imaging plate as well as the geometrical parameters of the BIX-3 diffractometer; Tanaka *et al.*, 2002). A total of 6584 independent reflections were obtained with an overall $R_{\rm merge}$ of 9.1% from 19 385 observed reflections. The completeness of the data set was 87.5% in the 50–1.60 Å resolution range and 66.0% for the outermost (1.66–1.60 Å) resolution shell.

The structure determination was performed with the refinement programs *X-PLOR* (Brünger, 1992), *CNS* (Brünger *et al.*, 1998) and the graphics programs *O* (Jones *et al.*, 1991) and *XtalView* (McRee, 1999). Neutron scattering lengths (*International Tables for Crystallography*, 1995, Vol. *C*, pp. 384–391) were used in these calculations and the parameters used in the dictionary files of *X-PLOR* were optimized for neutron scattering: whenever necessary, exchangeable H atoms were replaced with D atoms. The initial model was derived from the X-ray structure of mut-PfRd. The initial values for the R factor and $R_{\rm free}$ were 32.0 and 33.2%, respectively. Almost all of the H and D atoms were found in a neutron $|F_o| - |F_c|$ Fourier map before being included into the model and they were initially placed at calculated positions, except for the D atoms of OD and ND_3^+ functional groups and those of D_2O molecules: these D atoms were placed at sites located from neutron difference maps. In this manner, H and D atoms were gradually included in the model structure. At first, the H/D atoms of the main polypeptide chain (41 D and 5 H atoms) and H atoms whose positions could be predicted stereochemically (230 H) were added (R = 26.7%, $R_{\rm free}$ = 29.6%). Next, the H atoms of methyl groups (60 H) were added (R = 25.8%, $R_{\rm free}$ = 28.5%). Finally, the remaining D atoms (15 D) whose positions could not be predicted stereochemically were located from difference density maps and included in the structure. At the final refinement stage, the occupancies of the D atoms (the H/D-exchange ratios) of the amide bonds of the main chain were refined. Table 2 summarizes how the H and D positions were located. D_2O molecules were included very carefully only after the construction of almost the entire protein structure. Positive contours higher than the 3σ level in a neutron $|F_o| - |F_c|$ Fourier map were considered as candidates for water molecules and we judged whether they were correct or not by studying the hydrogen-bond patterns around them and also by considering the oxygen positions derived from the X-ray structure determination. 31 of the 53 D_2O molecules from the X-ray structure were ultimately included into the neutron structure and their D positions (when located) were refined with stereochemical restraints as described previously (Chatake *et al.*, 2003). Several D_2O molecules initially located from the X-ray analysis lacked neutron densities owing to disorder problems. While nine of the 31 D_2O molecules included in the neutron structure had the entire contour of

Table 2
Statistics regarding the location of H and D atoms.

Type of atom	Location method†	No. atoms	Average height (σ)	Percentage of atoms higher than		
				1σ	1.5σ	3σ
Protein C	X	250	4.1	98	96	77
Protein N	X	59	7.0	100	97	92
Protein O	X	80	3.7	94	93	71
Protein S	X	4	2.1	100	100	0
Fe	X	1	8.6	100	100	100
Side-chain O—D and N—D atoms	N	15	4.0	100	100	47
Main-chain amide H/D atoms	S	46	5.3	100	100	89
Non-methyl C—H H atoms	S	230	−2.4	97	85	22
Methyl C—H H atoms	S	60	−2.1	92	82	12
Solvent O atoms	X	29	3.1	100	100	41
Solvent D atoms	N	27	2.9	100	96	52
Missing D atoms of protein		12				
Missing D atoms of solvent		35				

† X, located from X-ray analysis; N, located from neutron difference map; S, the initial positions of these atoms were stereochemically calculated but their existence was subsequently verified from a neutron difference map.

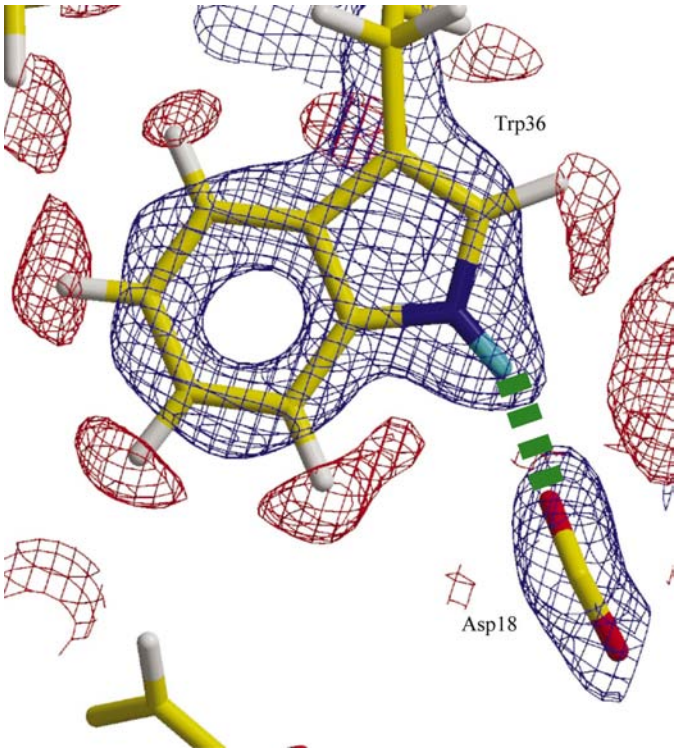

Figure 2
A final refined $2|F_o| - |F_c|$ neutron density map superimposed on the Trp36 residue. Blue and red contours show positive and negative densities, respectively. The green broken line shows a hydrogen bond between the N—D bond of Trp36 and the carboxyl group of Glu18. Note the positive contours of the N—D group and the entire D_2O molecule, as opposed to the negative contours of the H atoms of the C—H bonds.

three atoms (D—O—D), seven D_2O molecules were only partially located. Finally, 15 D_2O molecules only had a simple spherical contour corresponding either to a single O atom or to the center of gravity of a completely rotationally disordered water molecule. The final model included 31 water molecules located around the protein and of course also the Fe atom (R = 20.1%, R_{free} = 22.8%). The remaining 22 D_2O molecules found in the X-ray structure had diffuse neutron contours lower than the 3σ level and were consequently excluded from the neutron analysis. In addition, the two C-terminal residues which were disordered and were excluded from the X-ray model could not be located in the neutron analysis either, except for the backbone amide group of Glu52. Throughout the refinement, the atomic coordinates (x, y, z) and isotropic temperature factors (B_{iso}) for all atoms including H and D atoms were optimized by the least-squares technique using *X-PLOR* with the following restraints: E_{bond}, E_{angle}, $E_{dihedral}$, $E_{improper}$ and E_{vdW}. At the very end of the structural analysis, the positions of all atoms were checked individually on a graphical workstation display. Selected details of the neutron analysis are summarized in Table 1.

3. Results and discussion

3.1. Properties of mut-PfRd

Wild-type PfRd is stable for prolonged periods at 353 K at neutral pH and shows no detectable deterioration even after 5 d at this temperature (Jenney & Adams, 2001). The same was also true for the triple-mutant protein. However, when these proteins were incubated at 353 K at pH 2.0 there was a significant difference. Using visible absorption spectroscopy to assess the integrity of the protein (or more specifically the integrity of the iron site), the wild-type protein has a half-life of 208 s, but this decreases to 76 s for the triple mutant. In other properties, such as the reduction potential of the iron site (E_m = −40 mV) and the ability of the protein to bind (K_M = 26 μM) and to donate electrons (1430 units mg^{-1}) to an enzyme (NADH:rubredoxin oxidoreductase) from *P. furiosus*, the wild-type and mutant proteins were virtually indistinguishable (S. J. Simko & F. E. Jenney Jr, unpublished data).

3.2. Description of the neutron structure of mut-PfRd

Almost all the H and D atoms of mut-PfRd were observed in the 1.6 Å neutron-density map. A typical example showing the quality of the 1.6 Å neutron Fourier map is illustrated in Fig. 2, which displays the region near residue Trp36. The red contours around the indole ring indicate negative densities corresponding to the H atoms of C—H bonds, while blue contours correspond to positive regions, such as the D atoms of N—D bonds. The C, N and O atoms also appear as positive (blue) contours. Fig. 2 illustrates the fact that the N—H bond of tryptophan has exchanged with D when the protein was dissolved in D_2O (prior to crystallization), while the C—H bonds of this residue are unchanged. The neutron structure of mut-PfRd is composed of 394 non-H atoms, 15 D atoms, 46 D/H (partially deuterated) atoms and 290 H atoms. Mean-

while, 12 D atoms of the ND_3^+ groups of four of the five lysine groups (Lys2, Lys6, Lys28 and Lys50) are missing (Table 2), indicating that those amino groups are rotationally disordered. In order to confirm that the H and D atoms are truly present at their refined positions, an assessment procedure using a neutron Fourier map was carried out by measuring the peak height of each atom. In this assessment, a composite annealed $2|F_o| - |F_c|$ omit Fourier map was used to avoid bias from the model as much as possible (Brünger *et al.*, 1998). In fact, this was performed for every atom in the structure. The highest magnitude contour within a 0.5 Å radius from each refined atomic position was examined. As expected, in virtually every case the peak height of each atom correlated well with their neutron-scattering amplitude. The heights of the peaks for the S (positive) and H (negative) atoms are relatively small because of their low neutron-scattering amplitudes. Nevertheless, 96% of the H atoms have negative contours with magnitudes greater than the 1.0σ level (84% at the 1.5σ level), while all D atoms in the model have positive contours higher than 1.5σ. From this result, it can be concluded that the final model is reliable and precise.

Finally, it should be pointed out that almost the entire portions of two residues at the C-terminus are disordered in mut-PfRd, as they were in the wild-type protein (Kurihara *et al.*, 2001).

3.3. H/D distribution of the backbone N—H bonds

Prior to crystallization, the rubredoxin mutant used in this study was subjected to H/D exchange *via* dissolution in D_2O. The exposure to D_2O was continued during the crystallization process itself, which was carried out with a precipitant (sodium/potassium phosphate) also dissolved in D_2O[1].

This procedure produces a partially deuterated protein whose H/D-distribution pattern could, in principle, contain indirect information about the main-chain dynamics of a protein. H atoms in acidic or basic groups (in other words, those of O—H or N—H bonds) are potentially exchangeable for D atoms from D_2O in the mother liquor, while C—H bonds do not undergo exchange. At the H/D-exchangeable sites of the main chain (the amide N—H bonds), it was found that an average of 72.6% of the H atoms were replaced by D atoms. The scattering lengths of 100% D and 100% H atoms are very different ($b_D = 0.67$, $b_H = -0.37$) and thus the scattering length of a partially deuterated atom will range between these two extremes. The refined value of the scattering length of an H/D atom thus gives a direct measure of its H/D content. In our case, some H atoms of the amide bonds of the main chain (Val4, Cys5, Tyr12, Cys38, Ala43) still had negative contours in the neutron Fourier map (red dots in Fig. 3), indicating that the deuterium occupancies at those positions are less than 36%. It was concluded that those five N—H bonds (still mostly hydrogen) are not in contact with solvent D_2O molecules and that they are located in rigid parts of the protein which cannot easily exchange with deuterium. The H/D-exchange behavior of wild-type PfRd, which is remarkably similar to the results shown in Fig. 3, is also discussed in our report of the neutron crystallographic study of that protein (Kurihara *et al.*, 2004).

[1] The actual 'H/D-exchange time' is difficult to quantify. Initially, a solution of the protein in H_2O was concentrated, diluted with D_2O, concentrated again and the procedure repeated four times. This step took place in about 2 d, after which the rubredoxin solution was re-frozen and remained in a frozen state for a few months. It was then thawed out and crystals were grown over a period of several weeks at room temperature, after which the crystals were kept at room temperature for several months until data collection. Thus, the protein was in contact with D_2O for different periods of time, in solution and in the solid state, at room temperature and in a frozen state.

3.4. Comparison between neutron and NMR exchange analyses

The H/D-exchange behavior of wild-type PfRd has also been extensively analyzed by NMR spectroscopy (Hiller *et al.*, 1997; Hernandez *et al.*, 2000). In fact, extrapolation of the thermodynamic data derived from the kinetics of the most slowly exchangeable protons led to the conclusion that the

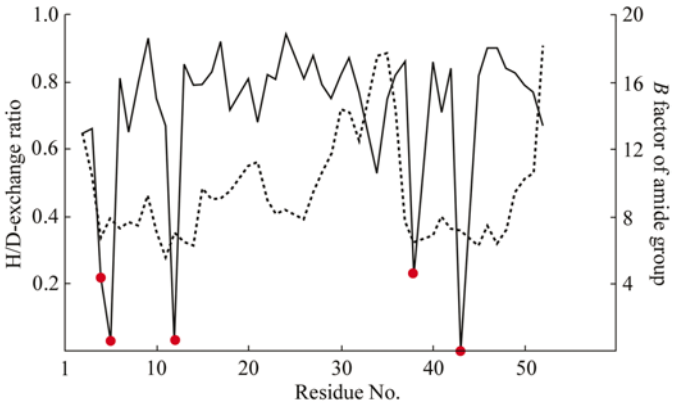

Figure 3
The deuterium-exchange ratios of the H atoms of the main-chain amide bonds, plotted against residue number. The red circles (corresponding to residues 4, 5, 12, 38 and 43) indicate the positions of N—H bonds whose H atoms have not been appreciably deuterated, implying that those H atoms are situated in structurally rigid parts of the molecule that are not exposed to the solvent. The dotted line corresponds to the trend of thermal parameters (*B* factors) of the H/D atoms of each amide group.

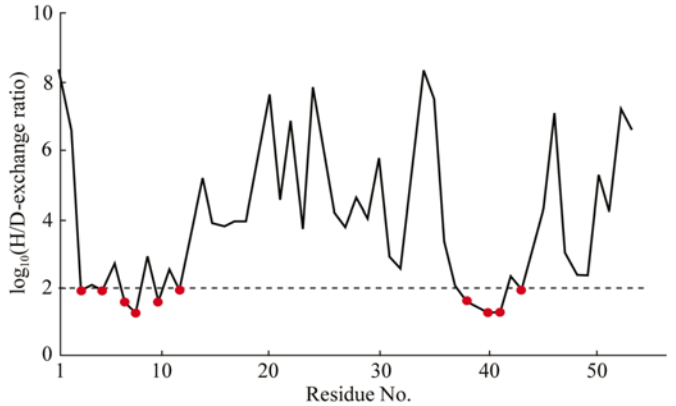

Figure 4
Results of the NMR H/D-exchange experiments (data taken from Hernandez *et al.*, 2000), showing the logarithm of exchange rates plotted against residue number. Note that the slowest-exchanging protons (red dots) are situated roughly in two regions, surrounding the Cys5/Cys8 and Cys38/Cys41 residues. In addition to this, there are two other minor 'islands of stability' near the Glu31/Leu32 and Phe48/Glu49 residues.

protein has an apparent melting temperature close to 573 K (Hiller *et al.*, 1997). A comparison of the data obtained by NMR with those obtained in the present study is shown in Figs. 3 and 4. For the NMR results, the rates for the various amide protons in the native protein range (remarkably) over eight orders of magnitude, with values for the most slowly exchangeable ones above $20\ M^{-1}\ s^{-1}$ (Fig. 4). Strictly speaking, the neutron and NMR data are not directly comparable since the former technique gives a dimensionless exchange ratio while the latter measures the exchange rate (in $M^{-1}\ s^{-1}$). Nevertheless, qualitative comparisons can be made between the two sets of results. For example, the most slowly exchangeable protons by NMR analysis (Fig. 4) are associated with the residues surrounding the four Cys residues (5, 8, 38 and 41; Hiller *et al.*, 1997; Hernandez *et al.*, 2000) and these also encompass the most rigid parts identified by neutron analysis, namely residues 4, 5, 12, 38 and 43 (Fig. 3). Clearly, at this level, the two techniques seem to identify the most stable parts of the protein. Interestingly, however, it can be seen from Fig. 4 that the NMR analysis also identifies two other 'islands of stability' in the wild-type protein near Glu31/Leu32 and near Phe48/Glu49, but these are missing (or not as pronounced) in the results of the neutron analysis of the mutant protein. The former of these could be directly related to the substitution of Leu32 for Ile in the triple mutant.

3.5. Comparison between the wild-type and the mutant structures

The hydrophobic core of mut-PfRd, which contains the three mutant residues (positions 3, 23 and 32), resembles that of wild-type PfRd, showing that the triple mutation did not significantly affect the core architecture. The three mutated residues retain almost the same atomic positions as those of the original three residues of wild-type PfRd. In two of the three (Ile23→Val23 and Leu32→Ile32), there are only very minor structural differences between mut-PfRd and PfRd (Fig. 5), mainly as a result of a methyl-group deletion (in the former case) and a methyl-group shift from C^{γ} to C^{δ} (in the latter case).

For the Trp3→Tyr3 substitution, however, substantial structural changes were indeed found, so that their hydrogen-bonding schemes are significantly different (Fig. 6). In wild-type PfRd (Kurihara *et al.*, 2001), the N_1—D_1 group from Trp3 and the O^{ε} atom from Glu14 make a direct hydrogen bond (D···O = 2.71 Å, N—D···O = 140°) (Fig. 6*a*). In contrast, in mut-PfRd the hydrogen bond between the third and 14th residues is absent and is replaced by a hydrogen bond between the O_4—D_4 group of Tyr3 and the O^{ε} atom of Glu30 (Fig. 6*b*). Moreover, the interaction between third and 14th side chains has been changed from a direct hydrogen bond in wild-type PfRd to an indirect hydrogen bond mediated by a D_2O molecule in mut-PfRd (Fig. 6*b*). The change in hydrogen-bonding patterns involving Glu14 may be especially important because earlier X-ray analyses have strongly implied the role of this residue in maintaining thermostability in rubredoxins.

In wild-type PfRd (Day *et al.*, 1992), the carboxylic group of Glu14 bridges three residues: the terminal amino group of Ala1, the indole N—D bond of Trp3 and the backbone amide

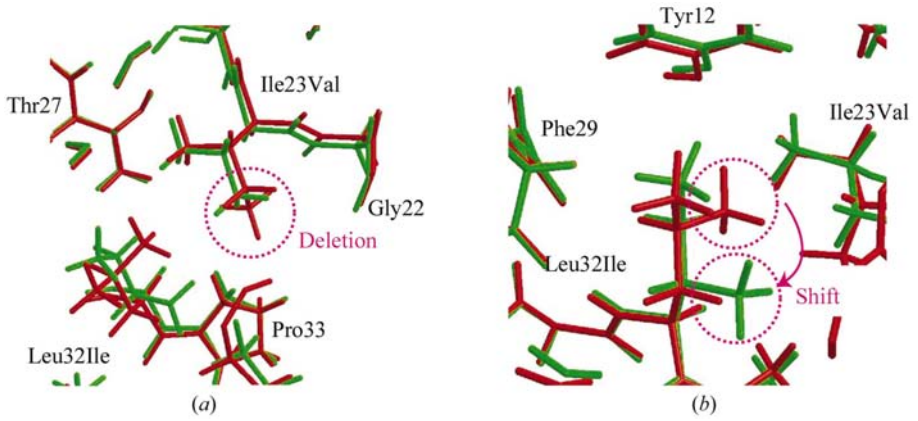

Figure 5
Three-dimensional structures around two of the mutated regions, Ile23→Val23 (*a*) and Leu32→Ile32 (*b*). A stick model of mut-PfRd (green) is superimposed on that of PfRd (red). Note that there is very little difference between the atomic positions in these two cases, other than the methyl-group shift shown at the right.

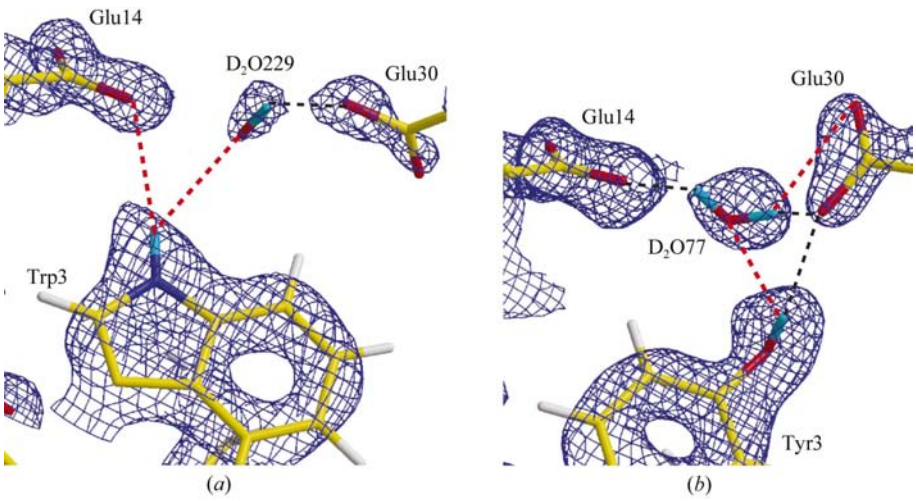

Figure 6
Maps around the third mutated region: (*a*) Trp3 in wild-type PfRd (Kurihara *et al.*, 2001) and (*b*) Tyr3 in mut-PfRd. The black and red broken lines show strong and weak hydrogen bonds, respectively. The blue contours correspond to positive neutron density regions. Note that Trp3 and Glu14 are directly hydrogen bonded in PfRd (*a*), whereas in mut-PfRd there is no direct hydrogen bond between Tyr3 and Glu14 (*b*).

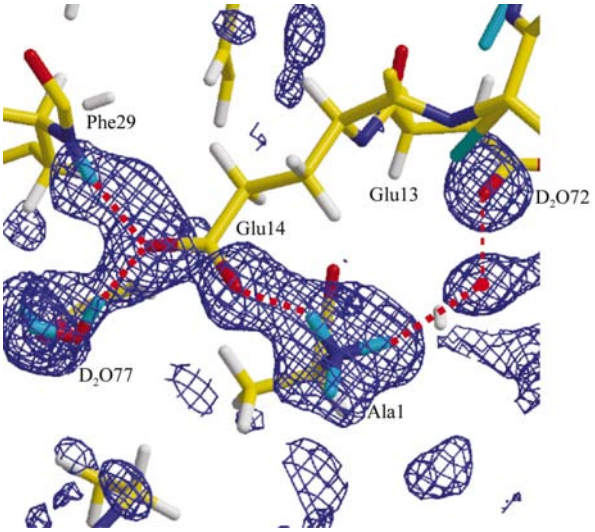

Figure 7
$|F_o| - |F_c|$ neutron-density map around the N-terminus, showing the tight arrangement of hydrogen bonds in this region and also showing the fully protonated nature of the terminal ND_3^+ group. Hydrogen bonds are shown as red dotted lines.

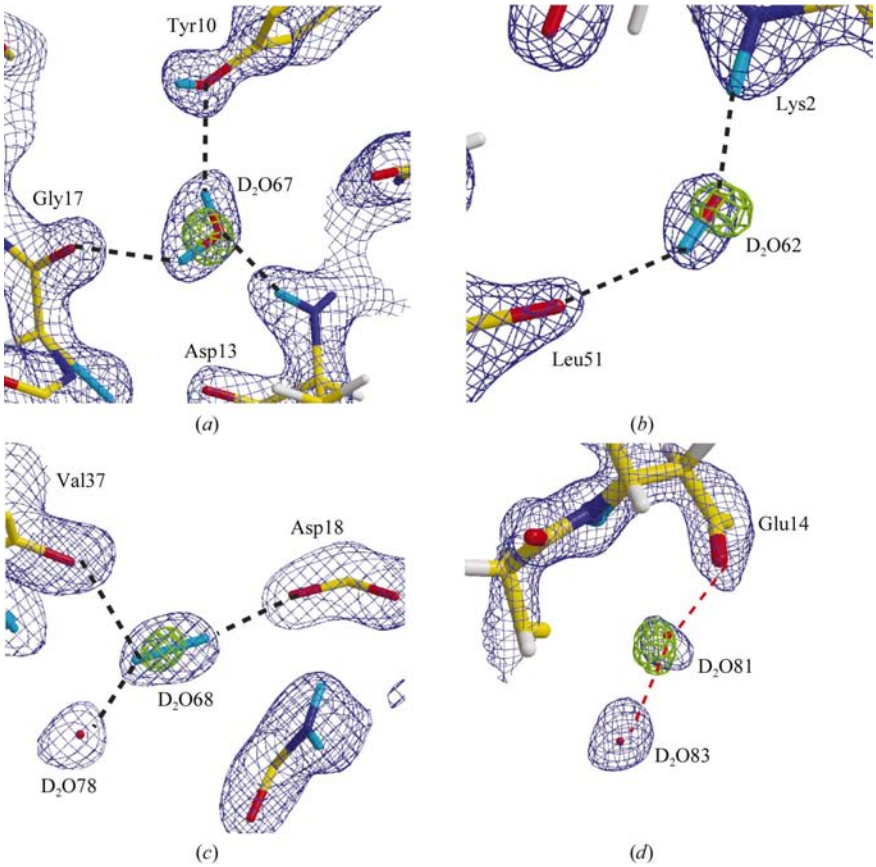

Figure 8
$2|F_o| - |F_c|$ maps of water molecules of hydration for the rubredoxin triple mutant observed by neutron protein crystallography. Examples shown are those of (*a*) triangular shape, (*b*) short ellipsoidal shape, (*c*) long ellipsoidal shape and (*d*) spherical shape. In these maps, the blue contours correspond to neutron peaks, while the green contours correspond to oxygen peaks from X-ray data. Observed (located) atoms from the neutron data are shown as stick diagrams, with the following color-coding scheme: C, yellow; N, dark blue/violet; O, red; D, light blue/cyan; H, white. Note that in (*a*) all atoms of the central D_2O molecule are visible (cyan/red/cyan), whereas in the other diagrams only some of the solvent atoms have been located: O, D in (*b*), two D in (*c*) and O only in (*d*).

group of Phe29. This can only occur in PfRd, because in mesophilic rubredoxins either Trp3 or Glu14 is replaced by other amino-acid residues: for instance, Trp3→Tyr3 and Glu14→Phe14 in CpRd. The entire N-terminus is a region rich in hydrogen-bonding interactions, which involve residues Phe29, Glu14, Asp13, the terminal ND_3 group and the aforementioned Tyr3 residue. Almost all of the D atoms involved in this elaborate chain of hydrogen bonds were found, as illustrated in Fig. 7, which shows the remarkable level of detail that can be displayed in a neutron Fourier map (including all three atoms of the ND_3^+ group). It is tempting to propose that the interactions of this region might account for the thermostability of PfRd and its variants (as compared with mesophilic rubredoxins), since they help to 'tie down' the N-terminus through the formation of this tight cluster of hydrogen bonds.

3.6. Water structure

The structural characteristics of protein hydration have been analyzed by several different kinds of techniques, such as X-ray crystallography (see Nakasako, 2001 and references therein), solution small-angle X-ray and neutron scattering (Svergun *et al.*, 1998), NMR spectroscopy (Otting *et al.*, 1991) and computational chemistry (Higo & Nakasako, 2002; Gu & Schoenborn, 1995). From single-crystal neutron diffraction, the hydration shell around proteins has also been discussed extensively by earlier investigators (Shu *et al.*, 2000; Habash *et al.*, 2000; Niimura *et al.*, 1997; Kossiakoff *et al.*, 1992; Finer-Moore *et al.*, 1992; Cheng & Schoenborn, 1990; Bon *et al.*, 1999; Harrison *et al.*, 1988; Schoenborn, 1988) and summarized in a recent review (Tsyba & Bau, 2002). Indeed, in a recent case the existence of various shapes of water peaks has been described (Habash *et al.*, 2000) and this topic has been discussed in great detail very recently (Chatake *et al.*, 2003). At 1.6 Å resolution, the present neutron study of a rubredoxin mutant has shown additional details that have not been clear before. Basically, we find four types of water molecules, as shown in Figs. 8(*a*)–8(*d*), classified according to appearance. Triangular-shaped peaks (Fig. 8*a*) represent the water molecules that are most ordered: in these cases, all three atoms (D, O, D) are apparent, arranged at the corners of an isosceles triangle. Next come ellipsoid-shaped peaks, which can be sub-classified as 'short' (Fig. 8*b*) or 'long' (Fig. 8*c*) and which correspond to water molecules with two ordered atoms. The difference between short and long ellipsoidal

peaks becomes apparent when one takes into account the oxygen positions as determined from X-ray data (green contours in Figs. 8*b* and 8*c*). In a 'short' ellipsoidal peak (Fig. 8*b*), the O atom is located at one end of the ellipsoid and the peak corresponds to an ordered D—O fragment, with the third atom (D) rotationally disordered and unobserved. In contrast, a 'long' ellipsoidal peak has the presumed oxygen position located in the middle (green peak in Fig. 8*c*), with the two ends of the peak located within hydrogen-bonding distances of hydrogen-bonding acceptors. Such 'long' ellipsoidal peaks thus correspond to the rare situations in which the D_2O molecule is rotationally disordered around the axis parallel to the D—D axis. Finally, spherical contours (Fig. 8*d*) correspond to only one ordered atom and these are usually coincident with the oxygen positions from X-ray Fourier maps: such peaks indicate water molecules that are completely rotationally disordered.

Table 3
Statistics of D_2O molecules in the neutron structure of mut-PfRd.

Classification	Triangular	Short ellipsoidal	Long ellipsoidal	Spherical	Missing†
No.	9	5	2	15	22
Average *B* factor (Å^2), neutron	22.0	33.2	31.9	45.7	—
Average *B* factor (Å^2), X-ray	20.6	25.9	23.0	31.6	36.6
Average No. of anchor points‡	2.4	1.6	2.0	0.4	
Labels used in Figs. 8 and 9	(*a*)	(*b*)	(*c*)	(*d*)	

† 'Missing' waters are those found from the X-ray analysis (as O atoms), but not found in the neutron analysis. ‡ An 'anchor point' of a D_2O solvent molecule is an atom that forms an identifiable hydrogen bond to a neighboring molecule. Thus, each D_2O molecule can only have a maximum of three anchor points even though in principle it can participate in as many as four hydrogen bonds.

The association between shape and disorder is summarized in Fig. 9. In the present room-temperature study, a total of 31 water molecules were definitively located in the crystal lattice, with nine, five, two and 15 belonging to the triangular, short ellipsoid, long ellipsoid and spherical classes, respectively. A total of 53 D_2O molecules were originally located in the X-ray structure; however, in the neutron study 22 of those solvent molecules had diffuse contours lower than the 3σ level in the $|F_o| - |F_c|$ Fourier map and hence were excluded from the neutron analysis. As shown in Table 3, the *B* factors of the D_2O molecules are related to the degree of order: small, intermediate and large *B* factors correspond to water molecules having triangular, ellipsoidal and spherical shapes in the neutron analysis, respectively, which correspond to D_2O molecules with increasing disorder. Moreover, the shape of a D_2O molecule is also strongly correlated with the number of hydrogen bonds attached to the atoms of the D_2O molecule (the number of 'anchor points'; see Table 3).

Other investigators (Habash *et al.*, 2000; Bon *et al.*, 1999; Schoenborn, 1988) have commented on the fact that water molecules around a protein appear to exist in shells, with the first hydration shell (near the protein) more ordered than succeeding shells. This suggestion is consistent with the hydration structure we find in the present neutron analysis of mut-PfRd. A more complete description of the hydration structure (in this and other small proteins) has been reported in detail elsewhere (Chatake *et al.*, 2003).

3.7. Directional character of hydrogen bonds

In the present study of mutant PfRd, 92 hydrogen bonds were found using the following definition: X—H(D)$\cdots Y$ (X, proton donor; Y, proton acceptor), distance[H(D)$\cdots Y$] < 3.0 Å, angle[X—H(D)$\cdots Y$] > 90°. Fig. 10 shows the distribution of proton acceptors (Y) in the hydrogen bonds. When Y is near a proton (*i.e.* when the hydrogen bond is strong), the hydrogen bond tends to be more linear (orange region in Fig. 10). As the distance becomes longer, the directional restraint becomes weaker (blue region in Fig. 10). This tendency coincides with the results from small-molecule crystallography. Using Pauling's classic definition of a hydrogen bond, a $d[H(D)\cdots Y]$ value smaller than 2.2 Å can be considered to be the upper limit of a covalent interaction (Pauling, 1939). Such a short hydrogen bond has a directional character (*i.e.* is approximately straight) owing to this covalency. However, electrostatic interactions can be found at longer distances. Pimentel & McClellan (1960) suggested a looser definition: they considered such a long-range interaction as 'a weak hydrogen bond'. Desiraju & Steiner (1999) further extended this concept and classified hydrogen bonds as strong and weak by the following definitions: strong hydrogen bond, 1.5 Å < d[H(D)$\cdots Y$] < 2.2 Å, 130° < angle[X—H(D)$\cdots Y$] < 180°; weak hydrogen bond, 2.2 Å < d[H(D)$\cdots Y$] < 3.0 Å, 90° < angle[X—H(D)$\cdots Y$] < 180°. In Fig. 10, strong and weak hydrogen bonds are indicated by orange and blue areas, respectively. The hydrogen bonds observed in mut-PfRd in the present study are assigned according to the definition of Desiraju & Steiner (1999).

There are 41 strong and 51 weak hydrogen bonds in an asymmetric unit. Table 4 shows the distribution of such bonds: strong hydrogen bonds were frequently observed in the inner regions of the protein. In particular, the percentage of strong hydrogen bonds is 67% among main-chain/main-chain interactions. Moreover, the strength of a hydrogen bond seems to be correlated with the thermal parameters of its constituent atoms. The average *B* factor of the three atoms (X, H/D, Y) participating in strong hydrogen bonds is 12.7 Å^2, while the average *B* factor for weak hydrogen bonds is 16.9 Å^2. The H/D-exchange ratio is also related to the type of hydrogen bond. Four out of the five amide groups (Val4, Cys5, Tyr12, Cys38) that have a low H/D-exchange ratio (shown as red dots in Fig. 3) make strong hydrogen bonds to backbone carbonyl groups. The one remaining amide bond (of Ala43) is hydrogen bonded to one of the S atoms in the $Fe(SCys)_4$ core. One could speculate that strong hydrogen bonds are involved in the main structural framework in a protein, while the weaker hydrogen bonds play a secondary role.

Table 4
Distribution of the hydrogen bonds in the rubredoxin mutant.

	Strong hydrogen bonds	Weak hydrogen bonds	% strong hydrogen bonds
Inner protein†	28 (20)	26 (10)	52 (67)
Water contacts‡	13	25	33
Total	41	51	

† Values in parentheses are for hydrogen bonds between main-chain and main-chain atoms. ‡ Includes protein–water and water–water hydrogen bonds.

3.8. Thermostability difference between wild-type and triple-mutant rubredoxins

The original motivation of this study was to provide some structural basis for rationalizing the thermostability difference between wild-type PfRd and the triple mutant, which is most pronounced at low pH (see above). Ideally, therefore, the structural comparison should have been made between two proteins that have been crystallized under acidic conditions. Unfortunately, this turned out not to be feasible. We have attempted to grow crystals of the two proteins at lower pH values and have failed in both cases: only thin needles (unsuitable for diffraction work) are formed around pH 5.0 and no crystals at all could be grown under more acidic conditions in our experience. Crystals of PfRd grow best under slightly basic conditions (pH 8.5). All we can do, therefore, is to compare the two structures at pH 8.5 and engage in some speculation as to what might happen at pH 2.0.

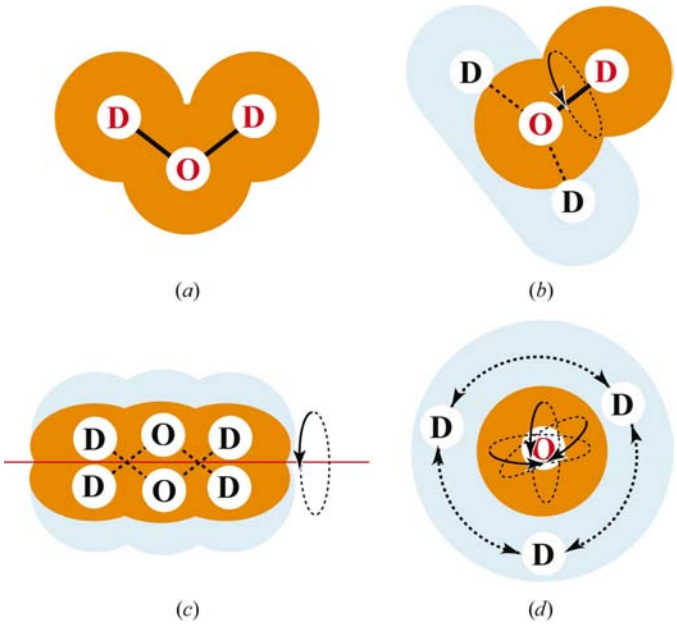

Figure 9
A schematic diagram showing the order or disorder of D_2O molecules corresponding to their individual shapes: (*a*) triangular, (*b*) short ellipsoidal, (*c*) long ellipsoidal and (*d*) spherical. The approximate peak shapes as seen in the neutron maps are shown as red–orange areas (regions of high positive contours) surrounded by, or adjacent to, cyan (or light blue) regions which correspond to low diffuse contours. The interpretations of these shapes are indicated by the 'O' and 'D' labels: ordered O and D atoms are shown in red, while disordered atoms are shown with black letters.

When the wild-type PfRd and the triple-mutant structures at pH 8.5 are compared, we found that two of the three mutated regions (residues 23 and 32) showed essentially no difference (Fig. 5), while the region near residue 3 (Fig. 6) did reveal some subtle but significant changes in the hydrogen-bonding pattern. In Figs. 6(*a*) and 6(*b*), both Glu14 and Glu30 are in their deprotonated (anionic) form. At pH 2, both carboxylate groups should be protonated and it is reasonable to assume that the hydrogen-bonding patterns involving Glu14 and Glu30 (now electronically neutral) would be weakened somewhat to the point at which the associated solvent molecules might even become detached. Indeed, in our earlier neutron analysis of lysozyme (Niimura *et al.*, 1997; Maeda *et al.*, 2001), it was established that one carboxylic residue (from Glu35) is hydrogen-bonded to a water molecule in its anionic state, but loses that water when the carboxylate group is protonated. If that were to happen here and a water molecule were to be lost, one could speculate that the interactions in the triple mutant (Fig. 6*b*) would be more strongly affected (since a bridging water molecule is necessary to hold residues 3 and 14 together), while the wild-type protein would be less severely affected, since in that case the hydrogen-bonding interaction between residues 3 and 14 (Fig. 6*a*) is direct and does not depend upon the presence of an intervening water molecule. This of course assumes that interactions involving residue Glu14 are crucially important in influencing the thermostability of PfRd (Fig. 7), a point we tried to make earlier in the discussion.

4. Conclusion

In the present neutron crystallographic analysis at 1.6 Å resolution, almost all positions of the H and D atoms of the triple mutant of rubredoxin from *P. furiosus* could be located and refined. We can summarize our conclusions as follows.

(i) We have shown that the H/D-exchange patterns are roughly comparable to the results from NMR spectroscopy

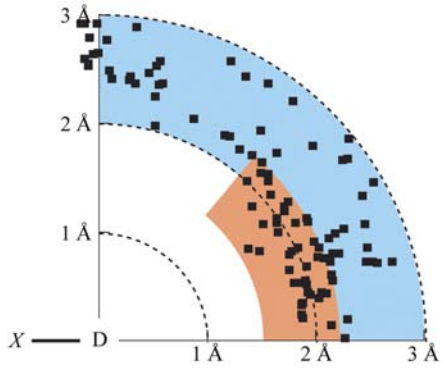

Figure 10
The distribution of Y atoms in X—H(D)$\cdots Y$ hydrogen bonds, with the position of the H(D) atom fixed at the origin. The component of H(D)$\cdots Y$ along the X—H(D) direction is plotted along the horizontal axis and the component of H(D)$\cdots Y$ perpendicular to X—H(D) is plotted in the vertical direction. The region of strong hydrogen bonds is indicated by the orange area, while weak hydrogen bonds are shown in the blue area.

and that the backbone N—H groups which show the lowest level of deuteration are near the FeS_4 redox center.

(ii) The 1.6 Å resolution structural analysis has allowed us to examine a protein structure in detail: for example, we were able to determine the orientations of all O—D bonds in the protein (*e.g.* the tyrosine residue shown in Fig. 6*b*), information which is not generally obtainable from X-ray data.

(iii) In the present analysis, we could determine not only the positions of many of the water molecules but also their orientation and dynamical behavior. We were able to classify D_2O peaks into three categories based on shape: triangular (all three atoms located), ellipsoidal (only two atoms ordered: O/D or D/D) and spherical (rotationally disordered water molecule).

(iv) The comparison between the present mutant and a wild-type protein shows significant differences arising from the Trp3→Tyr3 replacement: in particular, a direct hydrogen bond between the third and 14th residues in the wild-type protein (PfRd) has been replaced in the variant (mut-PfRd) with an indirect interaction mediated by a water molecule. While this does not provide any direct evidence to explain the thermostability difference between wild-type PfRd and the triple mutant at low pH, it does provide a structural foundation from which one can make extrapolations (from low to high acidity). One can then speculate that the ensuing changes in hydrogen-bonding pattern near residue 3 (at pH 2) might rationalize the observed thermostability difference.

We thank Dr Kaori Chiba and Dr Andreas Ostermann for suggestions and discussions about protein thermostability and protein crystallography. This work was supported in part by an 'Organized Research Combination System' Grant from the Ministry of Education, Culture, Sports, Science and Technology, Japan. RB and IT acknowledge support from the US National Science Foundation (grant CHE-98-16294) and the American Chemical Society (grant PRF-40715-AC3), while MWWA and FEJ wish to thank the Department of Energy (grant FG05-95ER20175) and the National Institutes of Health (grant GM-60329) for financial support.

References

Bau, R., Rees, D. C., Kurtz, D. M., Scott, R. A., Huang, H. S., Adams, M. W. W. & Eidsness, M. K. (1998). *J. Biol. Inorg. Chem.* **3**, 484–493.
Blake, P. R., Park, J. B., Bryant, F. O., Aono, S., Magnuson, J. K., Eccleston, E., Howard, J. B., Summers, M. F. & Adams, M. W. W. (1991). *Biochemistry*, **30**, 10885–10895.
Bon, C., Lehmann, M. S. & Wilkinson, C. (1999). *Acta Cryst.* D**55**, 978–987.
Brünger, A. T. (1992). *X-PLOR Version 3.1. A System for X-ray Crystallography and NMR*. Yale University Press, Connecticut, USA.
Brünger, A. T., Adams, P. D., Clore, G. M., DeLano, W. L., Gros, P., Grosse-Kunstleve, R. W., Jiang, J.-S., Kuszewski, J., Nilges, N., Pannu, N. S., Read, R. J., Rice, L. M., Simonson, T. & Warren, G. L. (1998). *Acta Cryst.* D**54**, 905–921.
Chatake, T., Ostermann, A., Kurihara, K., Parak, F. G. & Niimura, N. (2003). *Proteins*, **50**, 516–523.
Cheng, X. & Schoenborn, B. P. (1990). *Acta Cryst.* B**46**, 195–208.
Dauter, Z., Wilson, K. S., Sieker, L. C., Moulis, J. M. & Meyer, J. (1996). *Proc. Natl Acad. Sci USA*, **93**, 8836–8840.
Day, M. W., Hsu, B. T., Joshua-Tor, L., Park, J. B., Zhou, Z. H., Adams, M. W. W. & Rees, D. C. (1992). *Protein Sci.* **1**, 1494–1507.
Desiraju, G. R. & Steiner, T. (1999). *The Weak Hydrogen Bond* Oxford University Press.
Fiala, G. & Stetter, K. O. (1986). *Arch. Microbiol.* **145**, 56–61.
Finer-Moore, J. S., Kossiakoff, A. A., Hurley, J. H., Earnest, T. & Stroud, R. M. (1992). *Proteins*, **12**, 203–222.
Habash, J., Raftery, J., Nuttall, R., Price, H. J., Wilkinson, C., Kalb, A. J. & Helliwell, J. R. (2000). *Acta Cryst.* D**56**, 541–550.
Gu, W. & Schoenborn, B. P. (1995). *Proteins*, **22**, 20–26.
Harrison, R. W., Woldawer, A. & Sjolin, L. (1988). *Acta Cryst.* A**44**, 309–320.
Hernandez, G., Jenney, F. E. Jr, Adams, M. W. W. & Lemaster, D. M. (2000). *Proc. Natl Acad. Sci. USA*, **97**, 3166–3170.
Higo, J. & Nakasako, M. (2002). *Comput. Chem.* **23**, 1323–1326.
Hiller, R., Zhou, Z. H., Adams, M. W. W. & Englander, S. W. (1997). *Proc. Natl Acad. Sci. USA*, **94**, 11329–11332.
Jenney, F. E. Jr & Adams, M. W. W. (2001). *Methods Enzymol.* **334**, 45–55.
Jones, T. A., Zou, J. Y., Cowan, S. W. & Kjeldgaard, M. (1991). *Acta Cryst.* A**47**, 110–119.
Kossiakoff, A. A., Sintchak, M. D., Shpungin, J. & Presta, L. G. (1992). *Proteins*, **12**, 223–236.
Kurihara, K., Tanaka, I., Adams, M. W. W., Jenney, F. E. Jr, Moiseeva, N., Bau, R. & Niimura, N. (2001). *J. Phys. Soc. Jpn Suppl. A*, **70**, 400–402.
Kurihara, K., Tanaka, I., Adams, M. W. W., Jenney, F. E. Jr, Moiseeva, N., Bau, R. & Niimura, N. (2004). In the press.
Luzzati, P. V. (1952). *Acta Cryst.* **5**, 802–810.
McRee, D. E. (1999). *J. Struct. Biol.* **125**, 156–165.
Maeda, M., Fujiwara, S., Yonezawa, Y. & Niimura, N. (2001). *J. Phys. Soc. Jpn Suppl. A*, **70**, 403–405.
Mathieu, I., Meyer, J. & Moulis, J. M. (1992). *Biochem. J.* **285**, 255–262.
Nakasako, M. (2001). *Cell. Mol. Biol.* **47**, 767–790.
Navaza, J. (1994). *Acta Cryst.* A**50**, 157–163.
Niimura, N., Minezaki, Y., Nonaka, T., Castagna, J. C., Cipriani, F., Hoghoj, P., Lehmann, M. S. & Wilkinson, C. (1997). *Nature Struct. Biol.* **4**, 909–914.
Niimura, N., Karasawa, Y., Tanaka, I., Miyahara, J., Takahashi, K., Saito, H., Koizumi, S. & Hidaka, M. (1994). *Nucl. Instrum. Methods Phys. Res. A*, **349**, 521–525.
Otting, G., Liepinsh, E. & Wuthrich, K. (1991). *Science*, **254**, 974–980.
Otwinowski, Z. & Minor, W. (1997). *Methods Enzymol.* **276**, 307–326.
Pauling, L. (1939). *The Nature of the Chemical Bond.* New York: Cornell University Press.
Pimentel, G. C. & McClellan, A. L. (1960). *The Hydrogen Bond.* San Francisco: W. H. Freeman.
Schoenborn, B. P. (1988). *J. Mol. Biol.* **201**, 741–749.
Shu, F., Ramakrishnan, V. & Schoenborn, B. P. (2000). *Proc. Natl Acad. Sci. USA*, **97**, 3872–3877.
Svergun, D. I., Richard, S., Koch, M. H., Sayers, Z., Kuprin, S. & Zaccai, G. (1998). *Proc. Natl Acad. Sci. USA*, **95**, 2267–2272.
Tanaka, I., Kurihara, K., Chatake, T. & Niimura, N. (2002). *J. Appl. Cryst.* **35**, 34–40.
Tanaka, I., Niimura, N. & Mikula, P. J. (1999). *J. Appl. Cryst.* **32**, 525–529.
Tsyba, I. & Bau, R. (2002). *Chemtracts*, **15**, 233–257.
Zartler, E. R., Jenney, F. E. Jr, Terrell, M., Eidsness, M. K., Adams, M. W. W. & Prestegard, J. H. (2001). *Biochemistry*, **40**, 7279–7290.